HETC-HEDS Code Validation Using Laboratory Beam Energy Loss Spectra Data

Youssef M. Charara, Lawrence W. Townsend, *Senior Member, IEEE*, Tony A. Gabriel, Cary J. Zeitlin,
Lawrence H. Heilbronn, and Jack Miller

Abstract—**Recently, the Monte Carlo transport code HETC has been extended to include the interactions and transport of energetic heavy ions. Here, for the first time, we compare predictions of fragment production and energy loss with laboratory data measured at Brookhaven National Laboratory and at the National Institute of Radiological Sciences in Japan. Very good agreement is found for predicted and measured energy loss spectra for a variety of incident laboratory beams and targets.**

Index Terms—**Experimental validation, particle beams, radiation effects, radiation transport codes.**

I. INTRODUCTION

T O facilitate three-dimensional analyses of space radiation effects and protection scenarios for future space missions, the Monte Carlo radiation transport code HETC has been extended to include transport of energetic heavy ions, such as are found in the galactic cosmic ray spectrum. An event generator capable of providing nuclear interaction data for use in HETC was developed and incorporated into the code. The event generator predicts the interaction product yields and production angles and energies using nuclear models and Monte Carlo techniques. Testing and validation of the extended transport code has begun and preliminary comparisons with fragment yields reported previously [1]. In this work the current status of code modifications, which enable energetic heavy ions and their nuclear reaction products to be transported through thick shielding, are described. Here, for the first time, comparisons of energy loss spectra with data measured at Brookhaven National Laboratory and at the National Institute of Radiological Sciences

Y. M. Charara and L. W. Townsend are with the Nuclear Engineering Department, University of Tennessee, Knoxville, TN 37996-2300 USA (e-mail: ysharara@tennessee.edu; ltownsen@tennessee.edu; DrLTownsend@earthlink.net).

T. A. Gabriel is with Scientific Investigation and Development, Knoxville, TN 37922 USA (e-mail: jkgabrielta@earthlink.net).

C. J. Zeitlin was with Lawrence Berkeley National Laboratory, Berkeley, CA 94720 USA. He is now with Southwest Research Institute, Boulder, CO 80302 USA (e-mail: zeitlin@boulder.swri.edu).

L. H. Heilbronn was with Lawrence Berkeley National Laboratory, Berkeley, CA 94720 USA. He is now with the Nuclear Engineering Department, University of Tennessee, Knoxville, TN 37996-2300 USA (e-mail: lheilbro@utk.edu).

J. Miller is with Lawrence Berkeley National Laboratory, Berkeley, CA 94720 USA (e-mail: j_miller@lbl.gov).

in Chiba, Japan, which provide a more stringent test of the predictive accuracy of the code, are presented. Good agreement has been found between predicted and measured energy loss data for energetic heavy ions interacting in thick targets and their secondary fragments. We also note good agreement for fragment yields. Release of the code through the RSICC software repository at ORNL is planned for the near future.

II. HETC-HEDS CODE

A. Physics Description

The original version of HETC simulated the particle cascade by using Monte Carlo techniques to compute the trajectories of the primary particle and the secondary particles produced in nuclear collisions [2]. The particles considered by the original version of HETC (protons, neutrons, π^+, π^-, μ^+, or μ^-) could be arbitrarily distributed in angle, energy, and space. The energy loss of protons, charged pions, and muons due to the excitation and ionization of atomic electrons is treated using the well-established Bethe-Bloch stopping power formula based on the continuous slowing-down approximation. Multiple Coulomb scattering of primary particles is treated. Charged-pion decay in flight is taken into account. A π^+ which comes to rest is assumed to decay immediately into a μ^+ and a neutrino. A π^-, which comes to rest, may either decay or be captured by a nucleus. HETC does not transport π^0, although the energy, direction, and spatial point of the π^0 produced are included as part of the output. Muon decay in flight is taken into account using the known muon lifetime. Muons that come to rest are assumed to decay immediately. No information for the electrons, positrons, or neutrinos from muon decay is calculated. Elastic collisions of protons and π with all nuclei other than hydrogen are neglected at all energies. Pion production is based on the isobar model of Sternheimer and Lindenbaum. Only single- and double-pion production in nucleon-hydrogen collisions and single-pion production in p-nucleon collisions are accounted for. Nonelastic nucleon collisions and charged-pion collisions with hydrogen at energies above 3.5 GeV and 2.5 GeV, respectively, are treated by using calculational methods that utilize experimental data for the total nonelastic n-p, p-p, $\pi^+ - $ p, and $\pi^- - $ p cross sections and analytic fits to experimental data. The intranuclear-cascade evaporation concept of particle-nucleus interaction as implemented by Bertini is used to determine the effect of particle-nucleus collisions below 3.5 GeV for nucleons and 2.5 GeV for charged pions. Following the intranuclear-cascade the excitation energy left in the nucleus is treated using an evaporation model. The particles allowed during evaporation include protons, neutrons, d, ^{3}H, ^{3}He, and alphas. For high

energy (10–20 GeV) hadron-nucleus collisions, a complete intranuclear cascade does not develop. A multi-chain fragmentation model of hadron-nucleus collisions that has been developed and implemented in FLUKA, is used, with some modifications. To fill the gap between 3 to ~15 GeV, a scaling model is used. HETC used the combinatorial geometry package so virtually arbitrary geometries are allowed. Each particle in the cascade is followed until it eventually disappears by escaping from the geometric boundaries of the system, undergoes nuclear collision or absorption, comes to rest due to energy losses from ionization and excitation of atomic electrons, or, in the case of pions and muons, decays. Neutrons produced below a given cutoff, usually 20 MeV, and photons produced in the cascade or from deexcitation gammas are not transported. Instead, the information is stored for transport by codes such as MCNPX [3], MORSE [4], or EGS [5]. The complete cascade history file is provided.

Not included in the original HETC code was the transport and interactions of incident particles with $A > 1$. HETC has now been modified to include the transport of heavier nuclei. Included in this newer version of HETC, now called HETC-HEDS, are nucleus-nucleus cross sections, range-energy tables scaled from the proton data, and a nuclear collision module for heavy ion interactions [1], [6]. The nucleus-nucleus cross sections include the total, total reaction, and elastic scattering cross sections. The total reaction cross section is the cross section for all nuclear interactions that are not elastic scattering events. The elastic scattering cross section is the difference between the total cross section and the total reaction cross section. The nuclear collision module has two parts, one for elastic scattering events and one for fragmentation events. The fragmentation/spallation part is divided into two pieces as well, one for choosing the species of fragments produced and one for choosing those particles' kinetic energies and directions of travel. In non-elastic collisions, the resulting fragments, kinetic energies, and directions of travel are calculated for the projectile. Target quantities are obtained by interchanging the target and projectile. Choosing fragments produced in non-elastic collisions is accomplished by using a semiempirical model [7] to calculate heavy ion fragment production cross sections, where heavy is defined as lithium and heavier. Alpha fragmentation has been parameterized, and equations for helium-3, triton, and deuteron production cross sections taken from NASA TP 3285 [8]. Particle production due to helium-3 and triton breakup is based on their total proton and neutron production cross sections since each of these particles only have two reaction channels each. Deuteron breakup simply uses the total reaction cross section since it only has one reaction channel. The kinetic energy of fragmentation/spallation products is chosen using a microscopic model for the estimation of energy degradation in nucleus-nucleus collisions developed at the Naval Research Laboratory [9]. The momentum distribution of projectile fragmentation products is isotropic in a rest frame moving with nearly the projectile velocity. The momentum distribution of target fragmentation products is isotropic in a rest frame nearly at rest. Details can be found in [1] and [6]. Missing from the extension of HETC to HETC-HEDS are mesons produced in heavy ion collisions. Also missing are contributions from de-excitation gammas produced in the heavy ion frag-
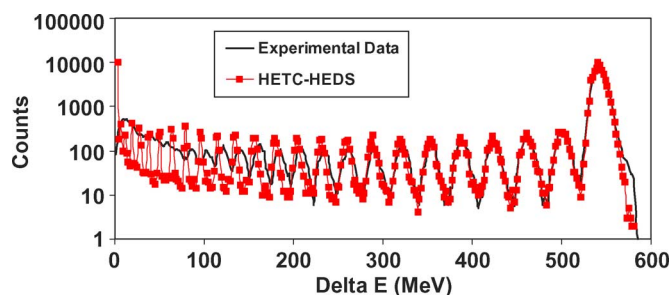

Fig. 1. Energy loss spectra in the thin silicon detector pair (nominal 1.88 mm total thickness) for 1.063 GeV/nucleon iron beam after passage through a 3.99 g cm^{-2} carbon target. There are 100 k events in the HETC-HEDS calculations and 91.2 k events in the experimental data.

mentation events. However, pion production and gamma decays in nucleon—nucleus collisions were included in the original HETC code. Recently models of pion production from heavy ion collisions have been developed for use in HETC-HEDS, but are not yet incorporated [10], [11].

HETC-HEDS runs quickly on a standard PC using a LINUX operating system. Typical run times for ~100,000 histories involving iron beams at 1 GeV/nucleon on targets several cm in thickness are ~5 minutes. Run times for incident ions lighter than iron are shorter. The file size for the complete history of the runs, however, can be quite large (up to ~1 GB).

III. BEAMLINE CONFIGURATIONS

Table I lists elements, material composition, location in the beamline, and dimensions for the laboratory beam experimental configurations used in the experimental runs discussed in this work. The elements are listed in the order that they appear in the beamline. Energy loss spectra are typically measured in PSD2 ("thin detectors") and in the thicker downstream detectors (3 mm or 5 mm thick detectors in the table). The detectors upstream of the target are used for triggering and, in the analysis, to select only events with a single primary ion incident on the target.

IV. REPRESENTATIVE RESULTS

A. 1 GeV/nucleon Fe Colliding With a C Target

Fig. 1 displays results for the energy loss spectrum measurements and calculations from a 1.063 GeV/nucleon beam of ^{56}Fe interacting with a 3.99 g cm^{-2} carbon target. The experiment was conducted at the Alternating Gradient Synchrotron (AGS) at Brookhaven National Laboratory. Due to energy losses in the components (trigger, PSD1) between the exit of the vacuum pipe and the target (1 MeV), the beam energy on target was 1.053 MeV [9], which was used in the calculations. The energy loss spectrum displayed here was measured in the thin Si detector pair (PSD2) in the beamline configuration listed in Table I. To account for the dead layers in the Si detectors and a nominal 5% uncertainty in calibration in the simulations, the thicknesses of the thin Si detectors were assumed to be 0.94 mm (total thickness of 1.88 mm). The experimental data plotted in the figure are from a run with a 2.66 cm target thickness (measured areal density of 3.99 g cm^{-2}) carried out in the 1995 Fe

TABLE I
BEAM LINE ELEMENTS, MATERIAL COMPOSITION, LOCATION IN BEAMLINE, AND DIMENSIONS FOR THE EXPERIMENTAL RUNS USED IN THIS WORK

Beam line element	Material	Distance (beam exit to center of element) (cm)	Thickness (cm)	Radius (or height for square target dimensions) (cm)
1.063 GeV/nucleon Fe + C, Al				
Tr 1	Si	18.1	0.03	0.98
Tr 2	Si	20.1	0.03	0.98
PSD1Y	Si	25.7	0.094	2.0
PSD1X	Si	27.7	0.094	2.0
Target	C, Al	33.0	2.66, 2.66	5.0, 12.0
PSD2Y	Si	62.2	0.094	2.0
PSD2X	Si	64.2	0.094	2.0
3mm1	Si	83.6	0.3	1.15
3mm2	Si	85.6	0.3	1.15
3mm3	Si	91.6	0.3	1.15
3mm4	Si	93.6	0.3	1.15
PSD3Y	Si	133.3	0.094	2.0
PSD3X	Si	135.3	0.094	2.0
600 MeV/nucleon O + CH$_2$				
PSD1Y	Si	18.0	0.094	2.0
PSD1X	Si	20.0	0.094	2.0
3mmu	Si	27.9	0.3	1.15
Target	CH$_2$	45.0	5.8	12.0
PSD2Y	Si	59.2	0.094	2.0
PSD2X	Si	61.2	0.094	2.0
5mm1	Si	123.3	0.5	1.9
5mm2	Si	125.3	0.5	1.9
3mm1	Si	188.1	0.3	1.15
3mm2	Si	190.1	0.3	1.15
800 MeV/nucleon Si + Sn				
T1	Si	91	0.03	0.98
d3mmu	Si	93	0.3	1.15
Target	Sn	97	0.5	10.0
d3mm1	Si	106	0.3	1.15
d3mm2	Si	108	0.3	1.15
PSD1Y	Si	110	0.094	2.0
PSD1X	Si	112	0.094	2.0
5mm1	Si	160	0.5	1.9
5mm2	Si	161	0.5	1.9
3mm3	Si	168	0.3	1.15
3mm4	Si	169	0.3	1.15
Scint 1	BC 401	174	0.5	12.7
Scint 2	BC 401	594	0.5	12.7
NaI	NaI	599	12.7	12.7

+ C experiments [12] and are similar those reported in Zeitlin *et al.* [12, Fig. 2]. Additional details of the experimental analyses are presented in [12]. Each peak in the spectrum represents a different elemental species. The highest energy peak (farthest right in Fig. 1) results from the iron isotopes. Hence, from right to left in the figure the peaks in order are Mn, Cr, V, Ti, etc. fragments. This particular experiment was unable to clearly resolve peaks for elements whose mass numbers were smaller than approximately half of the mass number of the incident ^{56}Fe. It is clear that the agreement between the HETC-HEDS simulation and the experimental measurements is quite good down to about S or Cl.

For these fragments, and lighter species, the peaks in the experimental data are broader and shifted to higher values of deposited energy, likely due to the detection of multiple fragments in coincidence. Table II displays fractional yields per incident

iron particle for the data presented in Fig. 1. The percent differences are calculated using

$$Diff = \left| \frac{Calc - Exp}{Exp} \right| \times 100\%. \qquad (1)$$

Note that the differences in predicted and measured yields are less than 17% for all elemental species listed. Most fragment yield differences were less than 10%. Comparable results are obtained for the yields of fragments for all other collisions presented herein.

B. 1 GeV/nucleon Fe Colliding With an Al Target

Figs. 2 and 3 display results for the energy loss spectrum measurements and calculations for a 1.063 GeV/nucleon beam of ^{56}Fe interacting with a 7 g cm^{-2} aluminum target. The experiment was conducted at the Alternating Gradient
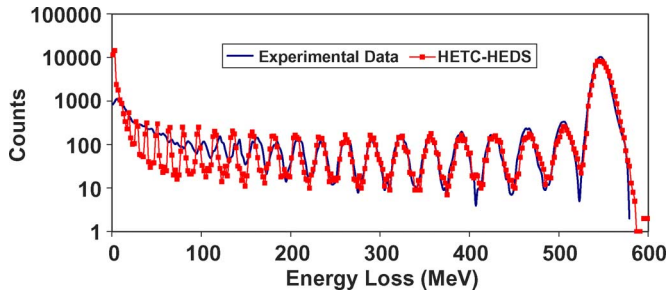
Fig. 2. Energy loss spectra in the thin silicon detector pair (nominal 1.9 mm total thickness) for 1.063 GeV/nucleon iron beam after passage through a 7 g cm^{-2} aluminum target.
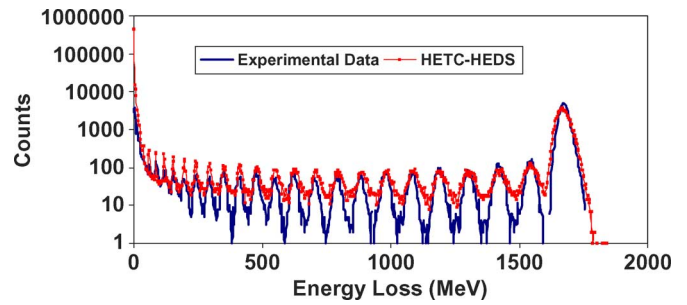

Fig. 3. Energy loss spectra in the thick silicon detector pair (nominal 5.7 mm total thickness) for a 1.063 GeV/nucleon iron beam after passage through a 7 g cm^{-2} aluminum target.

TABLE II
FRAGMENTATION YIELDS PER INCIDENT PARTICLE FOR 1.063 GeV/nucleon Fe COLLIDING WITH 3.99 g cm^{-2} C

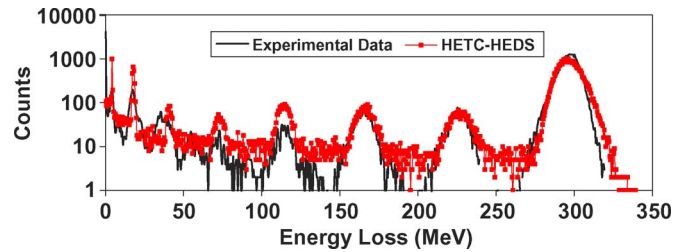|	HETC-HEDS Calculation	LBNL Experiment	Diff (%)
Fe	0.6770	0.7310	7.4
Mn	0.0212	0.0249	14.9
Cr	0.0153	0.0182	15.9
V	0.0127	0.0136	6.6
Ti	0.0116	0.0139	16.5
Sc	0.0104	0.0109	4.6
Ca	0.0098	0.0108	9.3
K	0.0092	0.0080	15.0
Ar	0.0092	0.0085	8.2
Cl	0.0078	0.0076	2.6
S	0.0078	0.0084	7.1
P	0.0071	0.0070	1.4

Fig. 4. Energy loss spectra in the thick silicon detector pair (nominal 9.1 mm total thickness) for a 600 MeV/nucleon oxygen beam after passage through a 5.31 g cm^{-2} polyethylene target.

Synchrotron (AGS) at Brookhaven National Laboratory. The energy loss spectrum displayed in Fig. 2 was measured in the thin Si detector pair (PSD2) in the beamline configuration listed in Table I. The energy loss spectrum displayed in Fig. 3 was measured in the first pair of thick Si detectors (nominal thickness 5.7 mm). The experimental data plotted in the figure are those reported by Zeitlin *et al.* [12]. As was the case for the C target results, this particular experiment was unable to clearly resolve peaks for elements whose mass numbers were smaller than approximately half of the mass number of the incident ^{56}Fe. The highest energy peak (farthest right in each of Figs. 2 and 3) results from the iron isotopes. Hence, from right to left in the figure the remaining peaks in order represent the Mn, Cr, V, Ti, etc. fragments. Again, it is clear that the agreement between the HETC-HEDS simulation and the experimental measurements is quite good down to about S or Cl. For lighter species, the peaks in the experimental data are again broader and shifted to higher values of deposited energy for the same reason as in the C target data.

C. 600 MeV/nucleon O Colliding With a Polyethylene Target

Fig. 4 displays results for the energy loss spectrum measurements and calculations for a 600 MeV/nucleon beam of ^{16}O interacting with a 5.31 g cm^{-2} polyethylene target. The energy loss spectrum was measured in the thick silicon detector pair 5 mm 1 + 2 in the beamline listed in Table I. From right to left in the figure, the peaks represent the yields of oxygen (Z = 8),

nitrogen (Z = 7), carbon (Z = 6), etc. The agreement between simulations with HETC-HEDS and the experimental data is very good for fragments with Z > 4. The agreement for peak locations for the fragments down to Z = 1 is also very good. Note, however, that there is a shoulder on the Z = 3 data peak, and an extra data peak between the Z = 3 and Z = 4 peaks. These are probably due to energy depositions by multiple helium fragments entering the detector and being recorded as a single particle. (For example, three helium fragments in coincidence have an effective charge of $\sqrt{2^2 + 2^2 + 2^2} = 3.46$.) The data were taken at the NASA Space Radiation Laboratory at Brookhaven National Laboratory in September 2004.

D. 800 MeV/nucleon Si Colliding With a Tin Target

Fig. 5 displays results for the energy loss spectrum measurements [13] and calculations for a 800 MeV/nucleon beam of ^{28}Si interacting with a 3.65 g cm^{-2} tin target. The energy loss spectrum was measured in the upstream thick silicon detector (d5mm1, nominal 4.85 mm thickness) in the beamline listed in Table I. The calculations and experimental data are normalized using: (the number of counts)/(Number of primary particles detected in d3mm 1 + 2). In Fig. 5, the Si peak has been suppressed. Thus, the right most peak representing the highest energy loss is the aluminum fragment peak. The remaining peaks from right to left represent the Mg, Na, Ne, F, etc. fragments. Note that the fragment peaks in the experimental data below nitrogen are not clearly present. Overall, for this system, the energies of the peaks for Z > 6 are in good agreement, but there are some discrepancies in the magnitudes of the calculated versus experimental peaks, except for the aluminum fragments. The
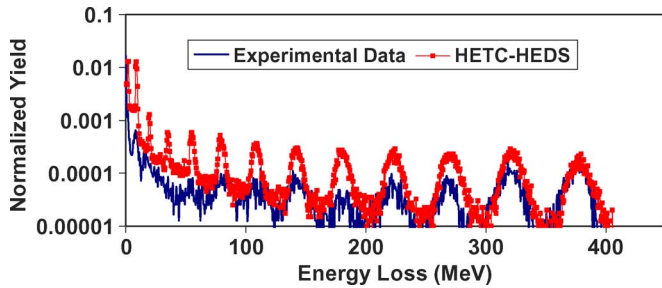
Fig. 5.   Energy loss spectra in the upstream thick silicon detector (d5mm1 nominal 4.85 mm thickness) for an 800 MeV/nucleon silicon beam after passage through a 3.65 g cm^{-2} tin target.

source of the disagreement in magnitudes is unclear and somewhat inconsistent, with the results of the fragment spectra and yield comparisons for the other systems presented herein.

V. CONCLUSION

For the first time, comparisons between HETC-HEDS code predictions and measured energy loss data for various ion beams relevant to galactic cosmic ray interactions are made and presented. These comparisons provide a more stringent test of the code predictions, beyond those provided by merely comparing particle yields. The overall agreement in peak heights, widths and locations between calculated and measured spectra and yields indicate that the calculated spectra closely reproduce the measured ones. Hence, the HETC-HEDS code is capable of providing reliable energy loss and particle yield estimates for laboratory and space radiation applications. Future validation includes comparing code predictions with measured spectra and radiation doses obtained from spaceflight data. Release of the code through the RSICC software repository at ORNL is planned.

REFERENCES

[1] L. W. Townsend, T. M. Miller, and T. A. Gabriel, "HETC radiation transport code development for cosmic ray shielding applications in space," *Radiation Protection Dosimetry*, vol. 115, no. 1–4, pp. 135–139, December 2005.

[2] K. C. Chandler and T. W. Armstrong, "Operating Instructions for the High-Energy Nucleon-Meson Transport Code, HETC," ORNL-4744, Oak Ridge National Lab.. Oak Ridge, TN, 1972.

[3] G. W. McKinney *et al.*, FNAL, "MCNPX overview," in *Proc. 2006 HSSW*, IL, Sep. 6–8, 2006, LA-UR-06-6206.

[4] M. B. Emmett, "MORSE-CGA, a Monte Carlo Radiation Transport Code With Array Geometry Capability," Oak Ridge National Lab., Oak Ridge, TN, ORNL-6174, Apr. 1985.

[5] A. F. Bielajew, H. Hirayama, W. R. Nelson, and D. W. O. Rogers, "History, Overview and Recent Improvements of EGS4," SLAC-PUB-6499 (NRC-PIRS-0436, KEK Internal 94-4) (Revised June 1, 1994).

[6] T. M. Miller and L. W. Townsend, "Comprehensive cross section database development for generalized three dimensional radiation transport codes," *Nucl. Sci. Eng.*, vol. 149, no. 1, pp. 65–73, January 2005.

[7] J. W. Wilson, J. L. Shinn, L. W. Townsend, R. K. Tripathi, F. F. Badavi, and S. Y. Chun, "NUCFRG2: A semiempirical nuclear fragmentation model," *Nucl. Instrum. Meth. Phys. Res.*, vol. 94, no. 1–2, pt. B, pp. 95–102, October 1994.

[8] F. A. Cucinotta, L. W. Townsend, and J. W. Wilson, "Description of alpha-nucleus interaction cross sections for cosmic ray shielding studies," TP-3285, National Aeronautics and Space Administration (NASA). Washington, DC, 1993.

[9] C. H. Tsao, R. Silberberg, A. F. Barghouty, and L. Sihver, "Energy degradation in cosmic-ray nuclear spallation reactions: Relaxing the straight-ahead approximation," *Astrophys. J.*, vol. 451, pp. 275–283, Sep. 1995.

[10] J. W. Norbury and L. W. Townsend, "Parameterizations of inclusive cross sections for pion production in proton-proton collisions. II. Comparison to new data," *Phys. Rev. D*, vol. 75, p. 034001, Feb. 2007.

[11] J. W. Norbury and L. W. Townsend, "Parameterized total cross sections for pion production in nuclear collisions," *Nucl. Instrum. Meth. Phys. Res. B*, vol. 254, no. 2, pp. 187–192, Jan. 2007.

[12] C. Zeitlin, L. Heilbronn, J. Miller, S. E. Rademacher, T. Borak, T. R. Carter, K. A. Frankel, W. Schimmerling, and C. E. Stronach, "Heavy fragment production cross sections from 1.05 GeV/nucleon ^{56}Fe in C, Al, Cu, Pb and CH_2 targets," *Phys. Rev. C*, vol. 56, no. 1, pp. 388–397, Jul. 1997.

[13] C. Zeitlin, A. Fukumura, S. G. Guetersloh, L. H. Heilbronn, Y. Iwata, J. Miller, and T. Murakami, "Fragmentation cross section of ^{28}Si at beam energies from 290A to 1200A MeV," *Nucl. Phys. A*, vol. 784, pp. 341–367, Mar. 2007.